RESEARCH PAPER

Investigation of the Effect of Welding Residual Stress on Natural Frequencies, Experimental and Numerical Study

Hussain Gharehbaghi[1] · Shahram Hosseini[1] · Rezvan Hosseini[2]

© The Author(s), under exclusive licence to Shiraz University 2022

Abstract
This paper investigates the effect of residual stresses resulting from welding on the values of natural frequencies of welded structures. First, two aluminum sheets constructed of the 6061-T6 alloy were argon welded together, and the residual stresses were measured via the hole-drilling method. Welding is carried out in two passes. Before starting the longitudinal weld, the beginning, the middle, and the end of the weld line are connected by spot welding to prevent the sheets from moving. The plate's natural frequency values without and with residual stress were retrieved using experimental modal analysis. The two aluminum plates are three-dimensional simulated in Abaqus finite element software, and residual stresses are extracted to validate the experimental results of the welding process. All the conditions in finite element analysis are similar to the welding conditions in the experimental specimen. The results demonstrate high accuracy in modeling the finite elements of the welding process. Then frequency analysis is performed numerically considering the residual stresses. Ultimately, the influence of residual stresses on natural frequency values was examined. The results illustrate that residual stress in the aluminum plate changes the natural frequency. This approach can be used as a non-destructive test to investigate the presence of residual stress in structures.

1 Introduction

Welding is very important in the aerospace, construction, and transportation industries. Welding has many applications in the connections of structures. One of the problems most industries face is residual stress due to the welding process. Residual stress in the areas around the weld can cause cracks to grow, so it is necessary to identify and study it in welded structures. There are several methods for measuring residual stress. A temperature field with a strong gradient is established in the parts in the welding process. Obtain temperature changes at any point during and after welding to predict the heat affected zone width, obtain the distribution of residual stresses weld, predict the macroscopic structure of different parts of the specimen, and predict the distortion

and deformation due to welding is essential (Million et al. 2005; Banno and Kinoshita 2022). Welding process due to the application of intense heat, deformation of the body and changes in the material's microstructure are one of the major causes of residual stress. Residual stress in structures can lead to distortion, unwanted and unauthorized deformation, or reduce metal structures' strength and useful life. Therefore, calculating the residual stresses resulting from the welding process is very important (Aliha and Gharehbaghi 2017). The presence of residual stresses in welded parts has adverse effects. Tensile residual stresses around the weld zone can cause cracks, corrosion, and structural failure (Murugan et al. 2001; Salameh et al. 2022).

There will be significant volumetric shrinkage during the cooling of aluminum and its alloys and reaching from the liquid stage to the solid stage. Traction and large expansion cause residual distortions in welded structures made of aluminum alloys. Therefore, the study of residual stress control and distortion of welded parts made of aluminum alloys is always an essential issue in welding engineering (Li et al. 2009). Measuring residual stress is very costly and time-consuming. Before choosing any measurement method,

✉ Hussain Gharehbaghi
  h.gharehbaghi@modares.ac.ir

1 Department of Mechanical Engineering, Tarbiat Modares University, Tehran, Iran

2 Department of Mechanical Engineering, Islamic Azad University South Tehran Branch, Tehran, Iran

the advantages and limitations should be examined to get the best result from the research. In previous studies, various methods have been developed to calculate residual stress. Nevertheless, this stress cannot be estimated directly and must be estimated using the residual strain determination tool.

Mechanical methods are necessarily destructive and cannot be used directly to measure residual stress intermittently. Due to the complexity of the welding process, analytical methods are often impractical, and practical methods cannot be used in the real specimen due to their destructive and costly nature. Accordingly, the best method for calculating the distribution of residual stresses is to use numerical analysis methods such as modeling and finite element analysis. Andersson (1978) investigated the residual stress distribution at the upper and lower surfaces of the base plate near the weld during the submerged arc welding process using the two-dimensional finite element method. Deng and Murakawa (2006) first experimentally measured the residual stress distribution in the weld zone using strain gauges installed near the weld zone. They then predicted residual stress distribution using Abaqus software and axial symmetry modeling. In recent years, many researchers have focused their efforts on modeling the welding process of aluminum alloys. Frigaard et al. (2001) created the thermal finite element model with a moving heat source and corrected their predicted temperature profiles by employing the experimental profiles obtained for 6082-T6 and 7108-T79 alloys. Khandkar et al. (2003) proposed a comprehensive model of the input heat based on welding tool torque and used it to model the temperature history of 6061-T651 aluminum alloy. Chen and Kovacevic (2003) acquired Ansys software to obtain the temperature distribution of 6061-T6 aluminum sheet during welding and compared it to their experimental results. Küçüköner et al. (2020) investigated the microstructure and mechanical properties of the AISI2205/DIN-P355GH steel joint by submerged arc welding. They bonded AISI 2205 duplex stainless steel and P355GH pressurized tank steel using additional metal and powder with similar parameters and a submerged arc welding method. These materials, which were welded using the SAW method, were tested for surface and subsurface defects using ocular, magnetic particle, and radiographic methods. Das Banik et al. (2021) studied the distortion and residual stresses in the weld joint of an austenitic stainless steel thick plate using experiments and finite element analysis. Arora et al. (2018) simulated the finite element of the residual stress due to welding in thin cylinders welded with a tungsten gas arc. Zhen et al. (2022), in their research, simulated the residual stress in the welding seam of aluminum alloy numerically based on computer simulation technology. Hu et al. (2019) conducted an experimental study of the residual stress test and finite element simulation using the nonlinear ultrasonic surface wave technique. Their primary purpose is to investigate the effect of residual stresses on the nonlinear behavior of materials to optimize a structural design. They experimented with three specimens of aluminum 7075 alloys under various residual stresses using nonlinear ultrasonic surface waves. Then, the residual stress distribution is simulated by shot pinning using the finite element method. They found that the nonlinear behavior of the material increases uniformly with increasing residual stress. The numerical results correspond to the experimental data quite well. The results indicated that the nonlinear surface ultrasound method has a high potential for detecting and evaluating residual stress. Liu et al. (2011) studied the measurement of residual stresses using nonlinear rail surface waves in shot-pinning specimens. Li et al. (2021) investigated the nonlinear behavior of anisotropic microplates with multi-layer electrostatically active residual stresses.

They investigated the behavior of anisotropic microplates and multilayer anisotropic microplates in the design and optimization of sensors and actuators. The results were then compared with isotropic materials and monolayer microplates. They presented a general reduced-order theory model considering both arbitrary multilayer properties and material anisotropy. The results were validated using experimental data and finite element simulations. Jiang et al. (2015) analyzed the vibrations of a piezoelectric nanowire based on a Green–Lagrange nonlinear strain equation. The effects of internal residual stress and geometric nonlinearity are evaluated.

In addition, the strain of the linear distribution with simply supported boundary conditions of the piezoelectric nanowire is investigated. The investigator used the method of the green–Lagrange nonlinear strain to obtain a set of equations governing transverse vibration through Hamilton's principle. Their results showed that internal residual stress could reduce the effect of residual surface stress and reduce the frequency significantly or change the frequency size dependence qualitatively. Penna et al. (2021) presented a review of the research and application of nanowire FG with geometric defects and initial axial force. They obtained that increasing the non-local parameter increases the nonlinear frequency for all nonlinear oscillator amplitudes and kinematic boundary conditions. The non-dimension nonlinear frequency increases with raising the initial axial prestress force for all non-local parameter values, regardless of the final condition. Verboven et al. (2006) discussed nonlinear distortions in modal testing vibrating automotive structures by testing. Ferhatoglu et al. (2018) analyzed the nonlinear vibrations of the structures with a new modal overlap method. They demonstrated that the new modal overlap method with hybrid mode shapes is an excellent reduction method for nonlinear dynamic analysis. Recent studies demonstrate that researchers have not considered the effect of

residual stress on natural frequencies. This problem is the main novelty of this research. First, two aluminum plates of AA6061-T6 are welded together using Argon (Tig). Using the central perforation method, longitudinal and transverse residual tensions are measured along the welding line. Then, using Abaqus software, this process is simulated. The distribution of residual stresses caused by welding with experimental results has been compared and confirmed by numerical simulation. Furthermore, due to the importance of the natural frequencies of aerospace structures, the effect of residual stresses on natural frequencies has been experimentally and numerically verified. Residual stresses can cause frequency changes, so this can be a simple method for confirming the presence or absence of residual stresses in the structure.

2 Experimental

2.1 The Manufacturing Procedure

In this research, the welding of AA6061-T6 aluminum sheet with final dimensions of 150×150 mm and a thickness of 6 mm has been studied. The argon welding process is used for the welding. The actual welding is performed in double pass using TIG welding using argon as shielding gas. This process is used ubiquitously for aluminum and its alloys (Díaz-Rubio et al. 2006). An electric arc connects a non-consumable tungsten electrode to the workpiece surface. The tip of the electrode, the puddle and the warm area around it are protected by inert gas (argon, helium, or a mixture thereof) escaping from around the electrode. From the available literature, the vital parameters affecting the quality characteristics of the process were identified as the welding current, voltage, welding speed and flow rate of shielding gas (Santhanakumar 2014). The welding parameters are considered such as the voltage of 12 (V), welding current of 120 (A), welding speed of 10 (cm/min) and flow rate of shielding gas of 15 (L/min). By using spot welding at the start and end of the weld line, the precise configuration of the joint was performed before the main welding. The photograph of the actual welded plates is shown in Fig. 1.

2.2 Residual Stress Measurement

In this study, using a hole-drilling method according to ASTM standard (E837) (2013) and a strain gauge (rosette with the FRS-2-23 model of TML company), residual stress changes at a depth of 1 mm from the workpiece surface are measured for each specimen and measured at three points according to Fig. 2. The selected points are in the center of the weld line, 15 and 30 mm from the center of the weld line, respectively.

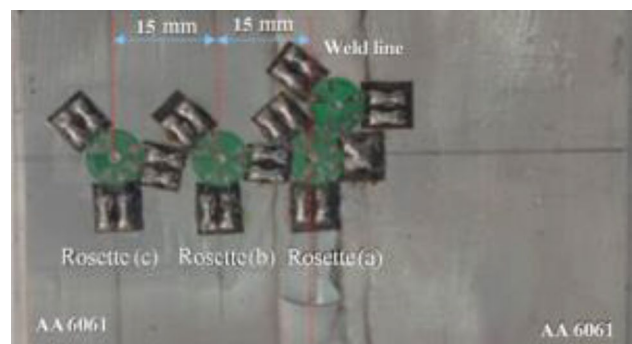**Fig. 1** The original pictures of weld plates

Fig. 2 Strain gauges on a welded sample

Hole-drilling is the most common method for determining residual stress. The advantages of this method are its low cost, ease of use, and accessibility. This method is classified as a semi-destructive method due to its size and depth (e; The diameter and depth of the hole are usually 0.8 to 3.2 mm). The steps used in order to perform the hole-drilling method according to the standard (ASTM E837-13a 2013) are: placing a 3-member strain gauge on the specimen, connecting and adjusting the strain gauges to the data device, and placing a device for drilling in the middle of the 3-member strain gauge, performing drilling operations, recording and converting results into residual stresses through existing relationships.

Flamen (Das Banik et al. 2021) showed that residual stress is created on the sides of the hole at low speeds in the drilling process. Therefore, the drilling speed in this experiment is estimated at 300,000 rpm, which was
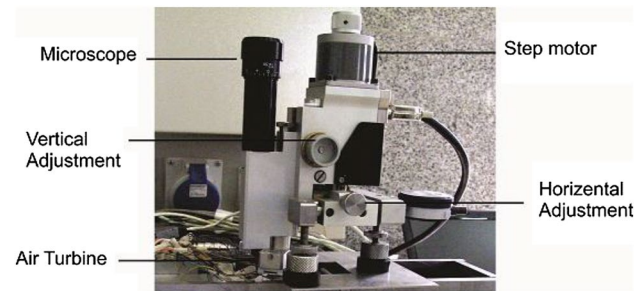
Fig. 3 The device used for high-precision stage punching

performed by the SINT MTS 3000 machine with high accuracy (refer to Fig. 3).

Residual stress on the sides of the hole is unavoidable due to the applied pressure and the heat generated in the drilling process. Non-uniform residual stress determination is performed according to the standard, with 20 drilling stages at a depth of 0.05 mm per stage. First, the readable strains from each strain gauge are used to define the new variables p, q, and t.

$$p = \frac{\varepsilon_1 + \varepsilon_3}{2} \tag{1}$$

$$q = \frac{\varepsilon_3 - \varepsilon_1}{2} \tag{2}$$

$$t = \frac{\varepsilon_1 + \varepsilon_3 - 2\varepsilon_2}{2} \tag{3}$$

where ε is the strain released. Then, using the equations obtained by Schajer (Schajer 1988), the combinations of P, Q, and T stresses were obtained according to Eqs. (4–6) and were related to the readable strains utilizing the calibration coefficients according to Eqs. (7–9).

$$P = \frac{\sigma_1 + \sigma_2}{2} \tag{4}$$

$$Q = \frac{\sigma_2 - \sigma_1}{2} \tag{5}$$

$$T = \tau_{13} \tag{6}$$

$$\bar{a}P = \frac{Ep}{1 + v} \tag{7}$$

$$\bar{b}Q = Eq \tag{8}$$

$$\bar{b}T = Et \tag{9}$$

where E is Young's modulus, and v is the Poisson's ratio of the part in question. $\bar{a}$ and $\bar{b}$ the calibration coefficients, σ and τ are the normal and shear stresses on the plane, respectively. The stresses and elasticity relations in each layer are obtained as Eq. (10). The k index corresponds to each layer.

$$(\sigma_{\max})_k, (\sigma_{\min})_k = P_k \pm \sqrt{Q_k^2 + T_k^2} = E\left[\frac{p}{\bar{a}(1+v)} \pm \frac{\sqrt{q^2 + t^2}}{\bar{b}}\right] \tag{10}$$

$$\beta_k = \frac{1}{2}\tan^{-1}\left(\frac{T_k}{Q_k}\right) = \frac{1}{2}\tan^{-1}\left(\frac{t}{q}\right) \tag{11}$$

2.3 Modal Analysis

The values of natural frequencies were calculated using a hammer and an accelerometer (see Fig. 4). The non-welded and welded specimens are considered simply supported boundary conditions. The excitation force is applied to the structure using the modal analyzer's hammer at the specified points. An accelerometer sensor then measures the resulting acceleration. The information received from the acceleration sensor is transformed into a frequency domain per unit of time using the Fourier series transformation.

3 Numerical Method (Welding)

Figure 5 indicates an aluminum sheet with a length of 150 mm, a width of 75 mm, and a thickness of 6 mm, produced by welding with longitudinal weld seams.

The welding process was assumed to be two-pass by the argon welding method. As illustrated in Fig. 5, the

Fig. 4 Measurement of the natural frequency of aluminum sheet using modal analysis
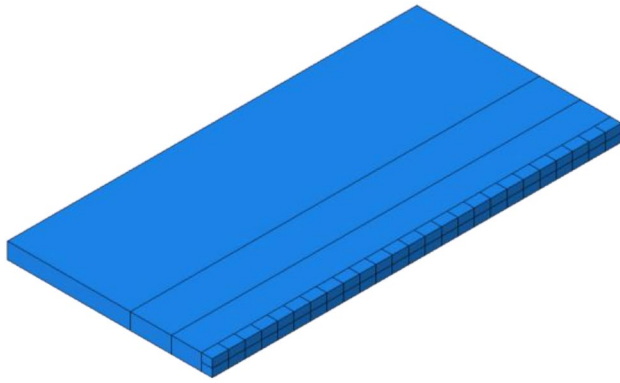
Fig. 5 Model plate with the longitudinal weld seam

butt connection is square. The plate is made of 6061-T6 aluminum alloy, and only half of the sheet is considered to reduce the model size and number of elements. Abaqus 14.2 finite element software was used to model the welding process in this research. Simulating the welding process is done simultaneously with thermal and mechanical analysis. For this purpose, a three-dimensional transient mechanical-thermal analysis is performed. The distribution of temperature and stress fields is obtained. The Goldak double ellipsoid model (Long et al. 2009) is used to model the heat source, shown in Fig. 6.

There are two models for kinematic hardening for metal cycle loading modeling in Abacus software. With a constant coefficient, the linear kinematic model approximates the hardening process. The linear kinematic stiffness coefficient is determined, C, in Eq. (12).

$$C = \frac{\sigma_y - \sigma_0}{\varepsilon^{pl}} \tag{12}$$

where σ_0, yield stress, σ_y, yield stress in plastic strain, ε_{pl}, plastic strain in the range. This model has reasonable results for minor strain ratios (less than 5%) based on physical principles.
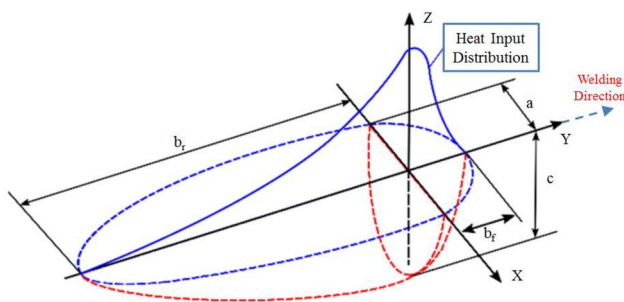
The nonlinear kinematic/isotropic model significantly predicts hardening, whereas it requires more detail for calculations and experiments. Therefore, linear kinematic stiffening has been used according to the strain values defined in the present study. The thermal and mechanical plate is considered a function of temperature, and the add or remove elements technique is used to model the filler material. All base metal components and weld metal elements formed due to material deposition must first be created to apply this approach. Consequently, welding metal elements are deactivated by multiplying the stiffness matrix of those elements into a minimal number. Similarly, when the elements are reactivated and the filler has precipitated after the heat source has passed, they are added to the model.

Instead, reactivating the elements means returning the stiffness matrices, mass, element loads, etc., to their original value. The finite element model constructed in this simulation is shown in Fig. 7. The first-order isoparametric brick elements have been used for analysis. Eight nodes with one degree of temperature freedom and 3 degrees of freedom of movement per node (C3D8T) were employed in the thermal analysis of the brick element. Due to the high-temperature gradients near the puddle and heat-affected zone, smaller elements in this area up to 10 mm from the welding line have been used. However, as the distance from the welding line increases, the size of the elements increases. The total number of elements in this modeling is around 9000. Due to the nonlinearity of the solution, a long time was required for the analysis. Therefore, changes in various parameters were ignored in modeling the welding process. Specific heat, thermal conductivity, density, latent heat, solidus and liquidus temperatures are essential to simulate the welding process's thermal behavior. The mechanical properties include Young's modulus, Poisson's ratio, yield stress, and thermal expansion coefficient, which are effective in thermoplastic analysis of the welding process. Properties materials are applied realistically and variable with temperature;
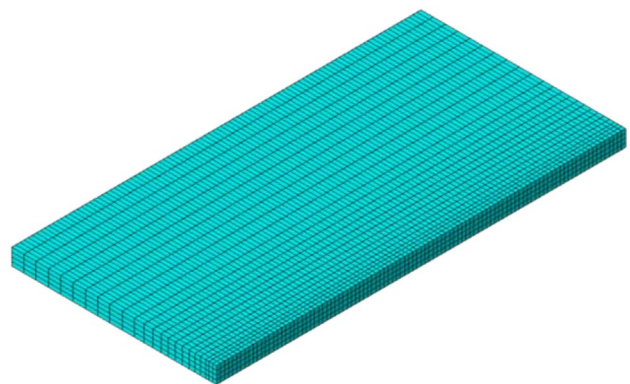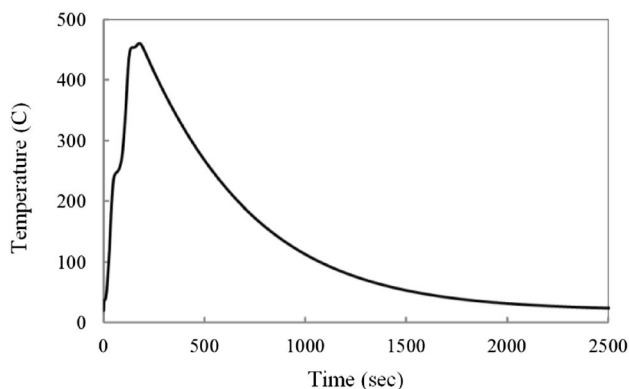

Fig. 6 Goldak's double ellipsoid model

Fig. 7 Three-dimensional finite element model of the aluminum sheet

Table 1 Relation between thermal and mechanical properties of aluminum 6061-T6 to temperature (Chao and Qi 1998; Aliha et al. 2013)

Thermal expansion coefficient (μ °C^{-1})	Young's modulus (GPa)	Density (kg/m^3)	Specific heat (J/kg °C)	Thermal conductivity (W/m °C)	Yield stress (MPa)	Poisson's ratio	Temp. (°C)
23.45	68.54	2685	945	162	277.7	0.33	37.8
23.61	66.19	2685	978	177	264.6	0.33	93.3
25.67	63.09	2667	1004	184	218.6	0.33	148.9
26.60	59.16	2657	1028	192	–	0.33	204.4
27.56	53.99	2657	1052	201	159.7	0.33	260
28.53	47.48	2630	1078	207	66.2	0.33	315.6
29.57	40.34	2630	1104	217	–	0.33	371.1
30.71	31.72	2602	1131	223	17.9	0.33	426.7

Fig. 8 Results of temperature history for the welding process

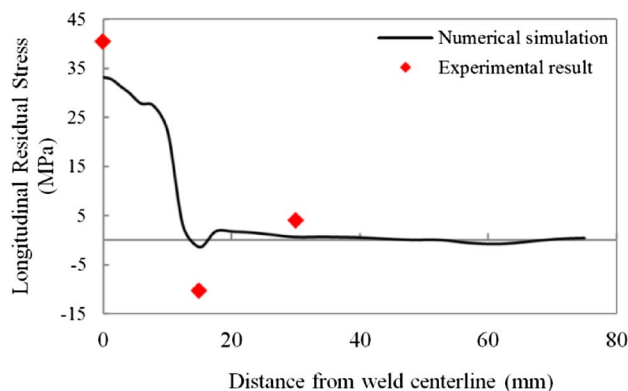**Fig. 9** The results of the longitudinal residual stress of the welding

consequently, the finite element analysis will be nonlinear, and the solution will be iterative (Zhu and Chao 2002).

The displacement of the nodes in the symmetry plane is perpendicular to the weld line to apply the boundary conditions. In addition, to prevent rigid movement of the system, the beginning and endpoints of the weld line are also clamped. A cube $1 \times 1 \times 1$ (mm) represents the melt area's size elements and the melt region's closeness. The level of adiabatic symmetry and the initial temperature of the plate are assumed to be equal to the ambient temperature of 20 °C. Table 1 illustrates the mechanical and thermal properties of the temperature-dependent 6061-T6 aluminum alloy utilized in this modeling. Furthermore, the latent heat is 384 kJ/kg, the liquidus temperature is 652 °C and the solidus temperature is 582 °C.

4 Discussion and Results

4.1 Welding Residual Stress

Figure 8 indicates the temperature history after 2500 s of the welding process at a point location 30 mm from the welding line's central and 150 mm from the beginning of welding.

The results for longitudinal residual stresses are shown (see Fig. 9). As observed in this process, the stresses surrounding the weld line are tensile, and the tensile residual stress is transformed to compressive residual stress at a distance of 13 mm from the center of the weld line. The finite element analysis results show that the maximum amount of tensile residual stress is about 34 MPa. Experimental results are presented at a depth of 0.1 mm from the surface. The maximum tensile stress at the center of the weld line is about 40 MPa. The small size of the welded part, the free part, the high heat input, and the two passes of the weld can be considered the reasons for reducing tensile residual stress in the present study. Residual stress is reduced by preheating before welding (Flaman et al. 1987; Fardan et al. 2021). The first pass in two-pass welding is a preheat of the second pass; Therefore, the residual stress in two-pass welding is less than in single-pass welding.

Suppose the sheets are clamped in the welding process. In that case, the amount of tensile residual stresses near the welding line will increase significantly (naturally, a significant percentage of the yield strength of aluminum material). This amount of residual stress will undoubtedly have a significant influence on the growth behavior of possible

cracks created in this area and will accelerate the growth of cracks and the destructive failure of cracks in the heat-affected zone.

4.2 Modal Analysis

4.2.1 Numerical Results

The sheet was subjected to frequency analysis in the presence of residual stresses caused by welding without taking residual stresses into account. The step related to frequency analysis is defined in numerical analysis to examine the residual stresses occurring from welding after the last step (cooling down) in the indicated study. Figure 10 showed the mode shapes of the welded sheet.

The results demonstrate that welding increases the stiffness of the sheet, which increases the natural frequencies. Table 2 exhibits the values for the first through third frequencies.

In fact, according to the nonlinear modal issues, residual stress is considered a tensile preload that can affect the natural frequencies of components and structures that have residual stress. As a result, by comparing the natural frequencies of the structure, it can understand the existence of residual stress.
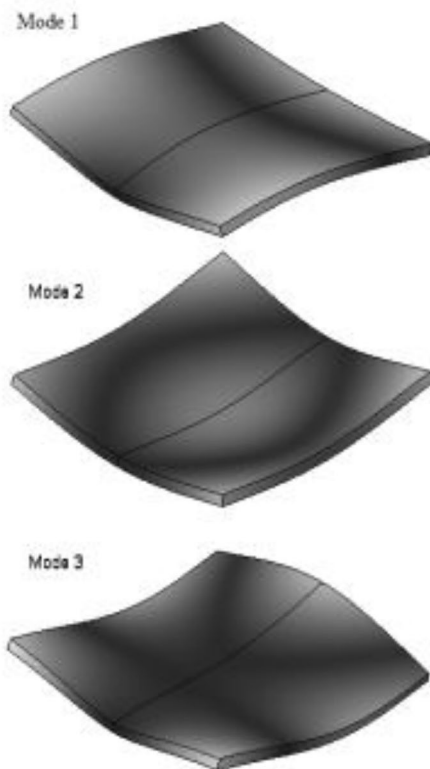
Table 2 Comparison of the natural frequencies of the sheet with the residual stresses from the welding and without of the residual stresses

	First frequency (Hz)	Second frequency(Hz)	Third frequency(Hz)
With residual stress	736.72	1609.0	1833.9
Without residual stress	730.26	1579.5	1812.1

4.2.2 Experimental Results

This section reviews the experimental results of modal analysis for welded and non-welded sheets. Figure 11 depicts the findings of the modal analyzer output (acceleration over time) for welded and non-welded sheets (MajidiRad and Yihun 2019).

The acceleration responses of the simple, welded sheets are converted to the frequency domain utilizing the fast Fourier transform, from which a frequency response diagram is obtained. Figure 12 shows the frequency response diagram for welded specimens. The difference between the two structures is visible in the first frequency mode (Fig. 13).

As can be seen, the first natural frequency was higher for the welded sheet. The presence of residual stresses in the plate increases the structure's natural frequency. The obtained experimental results confirm the numerical results, and the increase in frequency can be observed in the welded state.

5 Conclusions

In this research, the effect of residual stress on the natural frequency of aluminum sheets has been investigated experimentally and numerically. Detection of residual
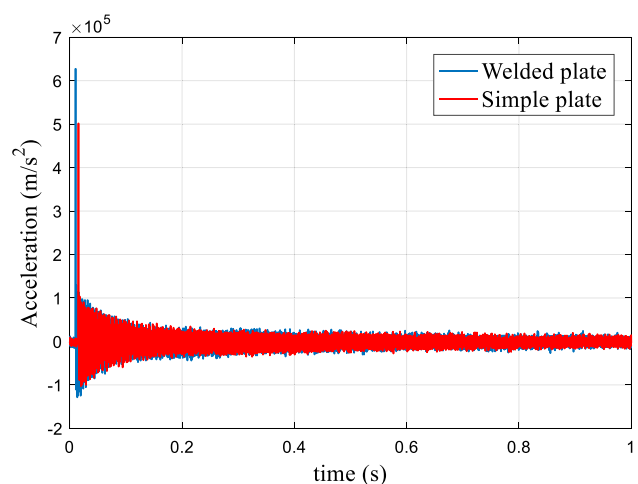

Fig. 10 Mode shapes of welded sheet

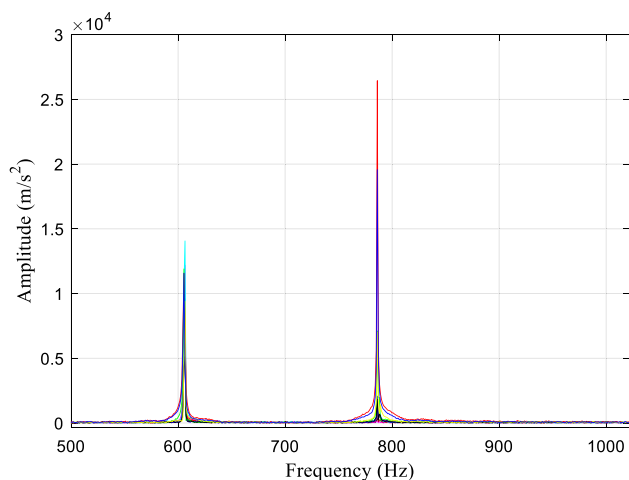**Fig. 11** The acceleration response for the welded and simple plate

Fig. 12 The frequency response function (FRF) diagram for the welded and simple plate
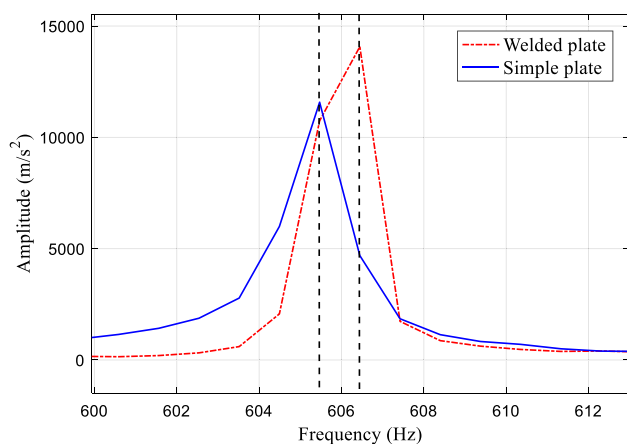

Fig. 13 The frequency response function (FRF) diagram for the first mode of a welded and simple plate

stress in different structures is essential. A novel approach for identifying the presence of residual stress is presented in this study. For this purpose, two aluminum sheets are considered, one of which the welding process has been done. Abaqus software for numerical analysis and modal analysis for experimental testing was considered. Numerical and experimental results revealed that the natural frequency could change in the presence of residual stress. The natural frequency values of welded and simple specimens differ by around 2%. This approach is one of the non-destructive tests used to identify residual stress in various constructions. Due to the high cost of investigating the presence of residual stresses resulting from welding, bending, and machining processes (which are often destructive), the study of frequency changes in the structure can indicate the presence of residual stresses in the structure.

Declarations

Conflict of interest The authors declare that they have no known competing financial interests or personal relationships that could have appeared to influence the work reported in this paper.

References

Aliha MRM, Gharehbaghi H, Ahangar RG (2013) Fracture study of a welded aluminum cylinder containing longitudinal crack and subjected to combined residual stress and internal pressure. In: 12th International Aluminum Conference, Canada

Aliha MRM, Gharehbaghi H (2017) The effect of combined mechanical load/welding residual stress on mixed mode fracture parameters of a thin aluminum cracked cylinder. Eng Fract Mech 180:213–228. https://doi.org/10.1016/j.engfracmech.2017.05.003

Andersson BAB (1978) Thermal stresses in a submerged-arc welded joint considering phase transformations. J Eng Mater Technol 100(4):356–362. https://doi.org/10.1115/1.3443504

Arora H, Singh R, Brar GS (2018) Finite element simulation of weld-induced residual stress in GTA welded thin cylinders. In: Reference module in materials science and materials engineering. Elsevier

ASTM E8374-13a (2013) Standard test method for determining residual stresses by the hole-drilling strain-gage method. ASTM International, West Conshohocken

Banno Y, Kinoshita K (2022) Experimental investigation of fatigue strength of out-of-plane gusset welded joints under variable amplitude plate bending loading in long life region. Weld World. https://doi.org/10.1007/s40194-022-01312-6

Chao YJ, Qi X (1998) Thermal and thermo-mechanical modeling of friction stir welding of aluminum alloy 6061-T6. J Mater Process Manuf Sci 7:215–233

Chen CM, Kovacevic R (2003) Finite element modeling of friction stir welding—thermal and thermomechanical analysis. Int J Mach Tools Manuf 43(13):1319–1326. https://doi.org/10.1016/S0890-6955(03)00158-5

Das Banik S, Kumar S, Singh PK, Bhattacharya S, Mahapatra MM (2021) Distortion and residual stresses in thick plate weld joint of austenitic stainless steel: experiments and analysis. J Mater Process Technol 289:116944. https://doi.org/10.1016/j.jmatprotec.2020.116944

Deng D, Murakawa H (2006) Numerical simulation of temperature field and residual stress in multi-pass welds in stainless steel pipe and comparison with experimental measurements. Comput Mater Sci 37(3):269–277. https://doi.org/10.1016/j.commatsci.2005.07.007

Díaz-Rubio FG, Franco DC, Sánchez-Gálvez V (2006) Fracture strength of welded aluminium joints in commercial road vehicles. Eng Fail Anal 13(2):260–270. https://doi.org/10.1016/j.engfailanal.2005.01.013

Fardan A, Berndt CC, Ahmed R (2021) Numerical modelling of particle impact and residual stresses in cold sprayed coatings: a review. Surf Coat Technol 409:126835. https://doi.org/10.1016/j.surfcoat.2021.126835

Ferhatoglu E, Cigeroglu E, Özgüven HN (2018) A new modal superposition method for nonlinear vibration analysis of structures using hybrid mode shapes. Mech Syst Signal Process 107:317–342. https://doi.org/10.1016/j.ymssp.2018.01.036

Flaman MT, Mills BE, Boag JM (1987) Analysis of stress-variation-with-depth measurement procedures for the residual stress measurement center-hole method of residual stress measurement. Exp Tech 11:35–37

Frigaard Ø, Grong Ø, Midling OT (2001) A process model for friction stir welding of age hardening aluminum alloys. Metall Mater Trans A 32(5):1189–1200. https://doi.org/10.1007/s11661-001-0128-4

Hu H, Zou Z, Jiang Y, Wang X, Yi K (2019) Finite element simulation and experimental study of residual stress testing using nonlinear ultrasonic surface wave technique. Appl Acoust 154:11–17. https://doi.org/10.1016/j.apacoust.2019.04.014

Jiang H, Wang C, Luo Y (2015) Vibration of piezoelectric nanobeams with an internal residual stress and a nonlinear strain. Phys Lett A 379(40):2631–2636. https://doi.org/10.1016/j.physleta.2015.06.006

Khandkar MZH, Khan JA, Reynolds AP (2003) Prediction of temperature distribution and thermal history during friction stir welding: Input torque based model. Sci Technol Weld Join 8(3):165–174. https://doi.org/10.1179/136217103225010943

Küçüköner H, Karakoç H, Kahraman N (2020) Investigation of microstructure and mechanical properties of AISI2205/DIN-P355GH steel joint by submerged arc welding. J Manuf Process 59:566–586. https://doi.org/10.1016/j.jmapro.2020.10.023

Li J, Yang J, Li H, Yan D, Fang H (2009) Numerical simulation on bucking distortion of aluminum alloy thin-plate weldment. Front Mater Sci Chin 3(1):84–88. https://doi.org/10.1007/s11706-009-0006-3

Li Z et al (2021) Nonlinear behavior analysis of electrostatically actuated multilayer anisotropic microplates with residual stress. Compos Struct 255:112964. https://doi.org/10.1016/j.compstruct.2020.112964

Liu M, Kim J-Y, Jacobs L, Qu J (2011) Experimental study of nonlinear Rayleigh wave propagation in shot-peened aluminum plates—Feasibility of measuring residual stress. NDT E Int 44(1):67–74. https://doi.org/10.1016/j.ndteint.2010.09.008

Long H, Gery D, Carlier A, Maropoulos PG (2009) Prediction of welding distortion in butt joint of thin plates. Mater Des 30(10):4126–4135. https://doi.org/10.1016/j.matdes.2009.05.004

MajidiRad A, Yihun YS (2019) Experimental and numerical investigation of residual stress stiffening influence on dynamic response of welded structures, vol 8. https://doi.org/10.1115/DETC2019-98123

Million K, Datta R, Zimmermann H (2005) Effects of heat input on the microstructure and toughness of the 8 MnMoNi 5 5 shape-welded nuclear steel. J Nucl Mater 340(1):25–32. https://doi.org/10.1016/j.jnucmat.2004.10.093

Murugan S, Rai SK, Kumar PV, Jayakumar T, Raj B, Bose MSC (2001) Temperature distribution and residual stresses due to multipass welding in type 304 stainless steel and low carbon steel weld pads. Int J Press Vessels Pip 78(4):307–317. https://doi.org/10.1016/S0308-0161(01)00047-3

Penna R, Feo L, Fortunato A, Luciano R (2021) Nonlinear free vibrations analysis of geometrically imperfect FG nano-beams based on stress-driven nonlocal elasticity with initial pretension force. Compos Struct 255:112856. https://doi.org/10.1016/j.compstruct.2020.112856

Salameh AA, Hosseinalibeiki H, Sajjadifar S (2022) Application of deep neural network in fatigue lifetime estimation of solder joint in electronic devices under vibration loading. Weld World. https://doi.org/10.1007/s40194-022-01349-7

Santhanakumar RAM (2014) Parameter design in fusion welding of AA 6061 aluminium alloy using desirability grey relational analysis (DGRA) method. J Inst Eng India Ser C. https://doi.org/10.1007/s40032-014-0128-y

Schajer GS (1988) Measurement of non-uniform residual stresses using the hole-drilling method. Part I—stress calculation procedures. J Eng Mater Technol 110(4):338–343. https://doi.org/10.1115/1.3226059

Verboven P, Guillaume P, Vanlanduit S, Cauberghe B (2006) Assessment of nonlinear distortions in modal testing and analysis of vibrating automotive structures. J Sound Vib 293(1):299–319. https://doi.org/10.1016/j.jsv.2005.09.039

Zhen W, Li H, Wang Q (2022) Simulation of residual stress in aluminum alloy welding seam based on computer numerical simulation. Optik 258:168785. https://doi.org/10.1016/j.ijleo.2022.168785

Zhu XK, Chao YJ (2002) Effects of temperature-dependent material properties on welding simulation. Comput Struct 80(11):967–976. https://doi.org/10.1016/S0045-7949(02)00040-8